# Arrays of Aligned Supramolecular Wires by Macroscopic Orientation of Columnar Discotic Mesophases

Hatice Duran,[†,⊥] Brigitte Hartmann-Azanza,[∥] Martin Steinhart,[∥,*] Dominik Gehrig,[†] Frédéric Laquai,[†] Xinliang Feng,[†] Klaus Müllen,[†] Hans-Jürgen Butt,[†] and George Floudas[‡,†,§,*]

[†]Max Planck Institute for Polymer Research, Ackermannweg 10, 55128 Mainz, Germany, [‡]Department of Physics, University of Ioannina, 451 10 Ioannina, Greece, [§]Biomedical Research Institute, Foundation for Research and Technology, Ioannina, Greece, [⊥]Department of Materials Science & Nanotechnology Engingeering, TOBB University of Economics and Technology, Söğütözü Cad. 43, 06560 Ankara, Turkey, and [∥]Institut für Chemie neuer Materialien, Universität Osnabrück, D-49069 Osnabrück, Germany

**ABSTRACT** Structure formation, phase behavior, and dynamics of mono-bromo hexa-*peri*-hexabenzocoronene (HBC-Br) are strongly affected by the confinement of cylindrical nanopores with rigid walls. Using self-ordered nanoporous anodic aluminum oxide (AAO)-containing arrays of aligned nanopores with narrow size distribution as a confining matrix, pronounced alignment of the HBC-Br columns along the nanopore axes was found to be independent of the pore diameter. Hence, arrays of one-dimensional supramolecular HBC-Br wires with the columns uniformly oriented along the wire axes on a macroscopic scale were obtained, unlike with discotics bearing smaller cores. The formation of the crystalline herringbone structure is shifted to lower temperatures in nanopores with diameters of a few hundred nanometers, whereas the formation of this low-temperature phase is completely suppressed when the pore diameter is below 20 lattice parameters. Moreover, the cylindrical confinement affects the disk axial dynamics as well as the distribution of relaxation times.

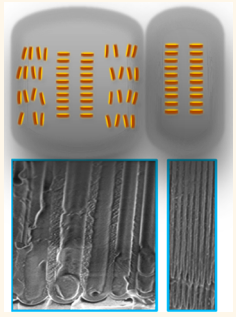

**KEYWORDS:** discotic liquid crystals · confinement · nanoporous aluminum oxide · supramolecular wires

Controlling the phase state and molecular packing/orientation of organic semiconductors through nanoconfinement is a challenging task. Discotic liquid crystals (DLCs) constitute a class of organic semiconductors where the phase state and the perfection in molecular packing is of paramount importance for device performance. Indeed, applications of DLCs in nanoscale conductive devices, organic field-effect transistors, and photovoltaic devices rely on the optimal stacking of the aromatic cores that allows for charge carrier mobility along the columnar axis (molecular wires).[1−4] Hexabenzocoronenes (HBCs) are an important class of DLCs. X-ray scattering revealed two main columnar structures in HBCs: first, a liquid-crystalline phase ($Col_h$) at higher temperatures composed of columns that are further organized in a hexagonal lattice; second, a crystalline phase ($C_r$) at lower temperatures composed of columns of tilted disks (*i.e.*, "herringbones") in a monoclinic unit cell. Extensive structural,[5,6] kinetic,[7,8] and dynamic[9,10] experiments in a series of dipole-functionalized HBCs revealed that the two phases possess not only distinctly different unit cells but also different dipolar and viscoelastic signatures.

Here, we explore the hard confinement of cylindrical nanopores having rigid pore walls to control (i) the thermodynamic stability of the $C_r$ and $Col_h$ phases, (ii) the columnar orientation, and (iii) the molecular dynamics in a mono-bromo hexa-*peri*-hexabenzocoronene (HBC-Br). HBC-Br has been extensively investigated in the bulk with respect to its self-assembly[5,6] (X-ray scattering), thermodynamics[5] (pressure, volume, temperature), dynamics[5] (dielectric spectroscopy, NMR, rheology), and the kinetics of structure formation.[7,8] We used self-ordered nanoporous aluminum oxide (AAO) templates[11−17] containing arrays of aligned cylindrical nanopores with sharp diameter distribution and uniform pore length to prepare aligned 1D HBC-Br nanowires. Earlier studies[18,19] on confined triphenylenes indicated that the formation of low-temperature phases can be suppressed by

* Address correspondence to gfloudas@cc.uoi.gr, martin.steinhart@uos.de.

Received for review July 2, 2012 and accepted October 26, 2012.

**Published online October 26, 2012**
**10.1021/nn302937t**

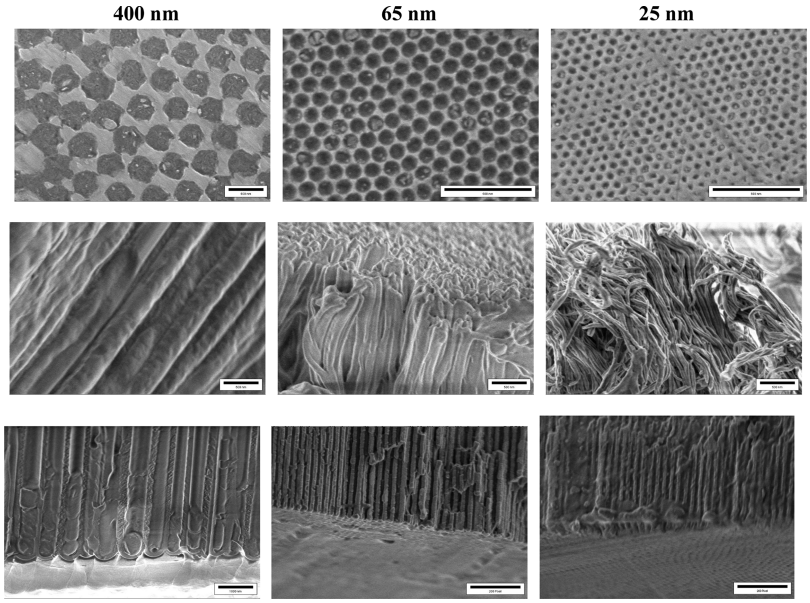


**Figure 1. Scanning electron microscopy images of self-ordered AAO after infiltration with HBC-Br having pore diameters of 400 (left column), 65 (middle column), and 25 nm (right column) with ~100 $\mu$m pore length. Images in the top (bottom) row refer to the top (bottom) view of HBC-Br embedded in AAO membranes. Images in the middle row refer to free-standing HBC-Br nanorods obtained by selective dissolution of the AAO membrane using dilute $H_3PO_4$ solution. The scale bar is 500 nm for all images.**

confinement. In addition, attempts for a possible uniaxial alignment of DLCs by confinement in hard templates[19,20] or nanogrooves[21] have been reported. However, in triphenylenes, the complete uniaxial alignment of the columns along the pore axes was hindered by the formation of a phase homeotropically anchored on the pore walls. In this respect, it is important to investigate the effect of discotics bearing larger cores. We have recently shown that 1D confinement affects the nematic-to-isotropic transition and completely suppresses the crystal-to-nematic transition in a calamitic liquid crystal.[16]

## RESULTS AND DISCUSSION

Self-ordered AAO with pore diameters of 25, 35, 65, 200, and 400 nm and a pore depth of ~100 $\mu$m was prepared following the procedures reported in the literature.[11−14] Infiltration of the HBC-Br was performed from solution as described in the Supporting Information. Figure 1 shows scanning electron microscopy (SEM) images of self-ordered AAO after infiltration with HBC-Br having pore diameters of 400, 65, and 25 nm, showing complete pore filling. The dynamics of HBC-Br was studied by dielectric spectroscopy (DS). DS is a versatile technique to probe the dynamics of molecules possessing a large dipole moment. The complex dielectric permittivity, $\varepsilon^* = \varepsilon' - i\varepsilon''$, where $\varepsilon'$ is the real and $\varepsilon''$ is the imaginary part, is generally a function of frequency $\omega$ and temperature $T$. Both, the orientation polarization of permanent dipoles and conductivity contribute to $\varepsilon^*$.[22] Orientational contributions can be fitted using the empirical equation of Havriliak and Negami (Supporting Information). In addition, the derivative of the dielectric permittivity[16,23,24] with respect to temperature, $d\varepsilon'/dT$, was employed to determine transition temperatures. Figure 2 (left) depicts the $d\varepsilon'/dT$ as a function of $T$ for bulk HBC-Br and HBC-Br located inside self-ordered AAO acquired under isochronal conditions ($f$ = 1154 Hz) at a cooling rate of 2 K/min. For bulk HBC-Br, a peak in the derivative indicated the transformation from the liquid-crystalline columnar $Col_h$ phase at high temperatures to the herringbone $C_r$ phase at lower temperatures. The corresponding $d\varepsilon'/dT$ cooling curve for the HBC-Br located inside self-ordered AAO with pore diameters of 400 and 200 nm also displays a peak, but its position is shifted to lower temperatures. No phase transition was detected for HBC-Br located inside self-ordered AAO with pore diameters $d$ = 65 nm and below, suggesting that the herringbone structure is completely suppressed when the pore diameter is below 20 lattice parameters of the monoclinic unit cell of the herringbone $C_r$ phase ($a$ = 2.82 nm).[5] Note also that previous studies on triphenylenes confined to the sponge-like pores of disordered nano- and mesoporous glasses revealed the suppression of the low-temperature phase.[18]

Differential scanning calorimetry (nitrogen atmosphere, heating and cooling rates 10 K/min) was carried out by cooling the samples to 153 K followed by heating to 423 K. The subsequent second cooling and heating scans were used to determine transition temperatures $T_{C_r/Col_h}$ and the associated heats of fusion. The pore diameter dependence of $T_{C_r/Col_h}$ obtained from DS and DSC (Supporting Information, Figure S1) is summarized in a pertinent "phase diagram" (Figure 2,

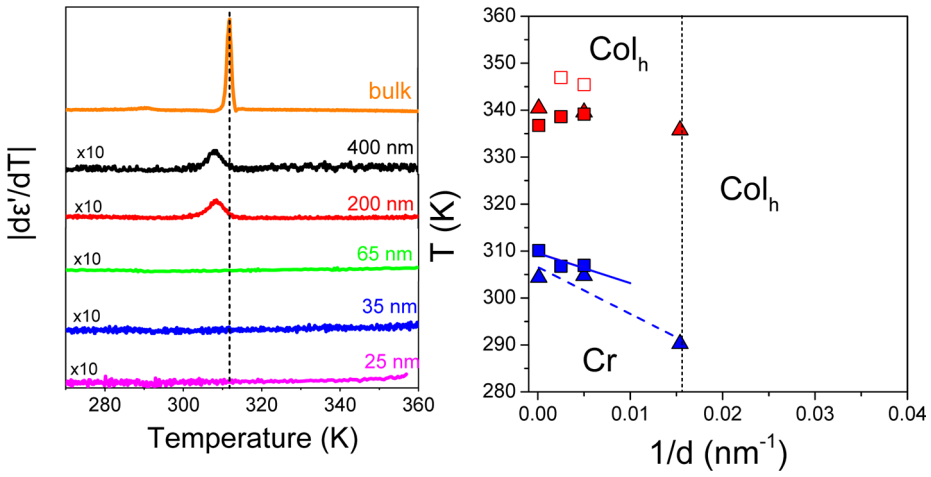


**Figure 2. (Left) Absolute derivative of the dielectric permittivity as a function of temperature for the bulk HBC and for HBC located inside self-ordered AAO on cooling. All measurements were obtained at a rate of 2 K/min at a frequency of 1154 Hz. The vertical line indicates the $Col_h$ to $C_r$ transition temperature of bulk HBC. (Right) Dependence of the $Col_h$ to $C_r$ transition temperatures of bulk HBC and of HBC located inside self-ordered AAO plotted as a function of the inverse pore diameter. The red (blue) symbols correspond to the transition temperatures on heating (cooling) and are obtained by DS (squares) and DSC (triangles). The solid and dashed lines represent linear fits to the DS and DSC data obtained on cooling.**

right). DS results revealed a reduction in $T_{C_r/Col_h}$ on cooling in confinement that can be parametrized as $T_{C_r/Col_h} = 309.5 - 640/d$, where $d$ is in nanometers. DSC yielded a steeper pore diameter dependence $T_{C_r/Col_h} = 306.6 - 990/d$. The reduction in $T_{C_r/Col_h}$ can be explained by a decreasing density of the columns in the vicinity of the pore walls. According to the Clausius–Clapeyron equation[5] describing the effect of pressure on $T_{C_r/Col_h}$ according to $dT_{C_r/Col_h}/dP = 0.256$ K/MPa, a reduction in $T_{C_r/Col_h}$ by ~5 K requires a reduction in pressure by 20 MPa that—as can be estimated from the known equation of state for HBC-Br—results in a decrease in density of 0.01 g/cm$^3$ (corresponding to the relative reduction in density of about 1%). Such a (small) reduction in density suffices to explain the reduction in $T_{C_r/Col_h}$. In this view, the geometric constraint imposed by the hard confining AAO pore walls is equivalent to external pressure.

Wide-angle X-ray scattering (WAXS) yields complementary information on the phase state as well as on the columnar orientation in the $Col_h$ phase. Figure 3 shows Θ/2Θ scans of the $Col_h$ phase taken at 353 K using the geometry described previously.[16,17,19] The AAO surface was oriented perpendicularly, and the AAO nanopore axes were oriented parallel to the scattering plane. Thus, only sets of lattice planes oriented normal to the AAO pore axes and parallel to the AAO surface contributed to the scattered intensity. The WAXS patterns of liquid-crystalline columnar HBC-Br contained a strong intracolumnar (001) reflection from columns oriented along the AAO nanopore axes and a weaker intercolumnar (100) reflection from columns oriented perpendicular to the AAO nanopore axes. The intensity of the intercolumnar (100) reflection systematically decreases with decreasing pore size, and for AAO pores with $d$ = 25 nm, the (100) reflection is completely

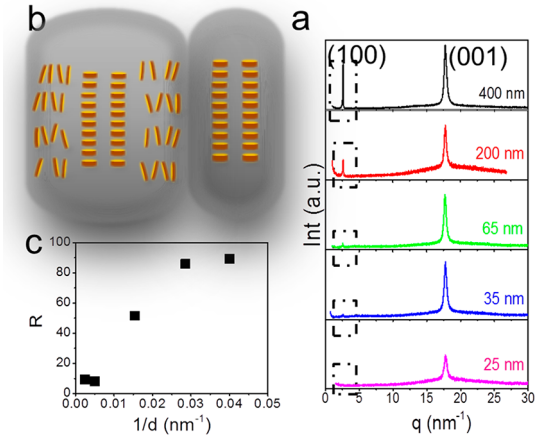


**Figure 3. (a) Results from the Θ/2Θ scans with the template surface oriented perpendicularly to the plane of the incident and scattered X-ray beam obtained at 353 K corresponding to the $Col_h$ phase. The diffractograms depict the strong intracolumnar (001) reflection from columns oriented along the nanopore axis, and for the larger pores, the intercolumnar (100) reflection is from columns oriented perpendicular to the nanopore axis. (b) Schematic depicts the selective orientation of columns for the smaller nanopores depicting the two possible columnar orientations; one with columns oriented along the AAO pore axes and one oriented perpendicular to the pore axes. (c) Dependence of the intensity ratio $R$ of the intracolumnar to the intercolumnar peaks on the inverse pore diameter.**

absent. The correlation lengths along the (001) direction derived from the intramolecular peak using the Debye–Scherrer equation range from 16 to 20 nm; that is, the HBC-Br stacks comprise about 40–60 molecules.

To further investigate the apparent texture, we conducted Schulz scans[25] as described previously.[19,26] Schulz scans were measured with fixed Θ and 2Θ angles by tilting the AAO about the Ψ axis by a tilt angle Ψ. The Ψ axis lay in the scattering plane and was oriented

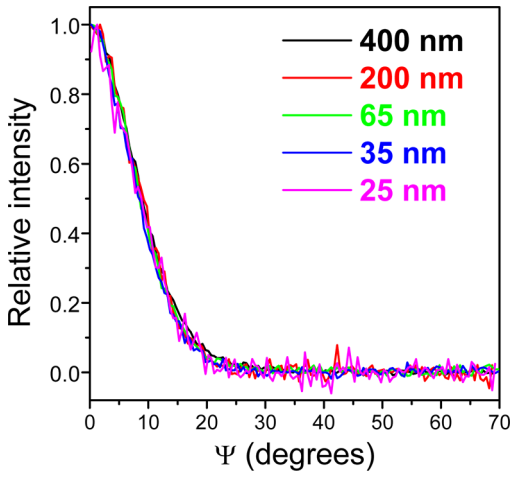


**Figure 4. Comparison of the normalized Schulz scans for the intracolumnar (001) peak for all AAO diameters made at 353 K. The value of the calculated Hermans orientation parameter of ≈0.95 suggests an alignment of the columns along the AAO pore axes.**

perpendicular to the Θ/2Θ axis. The Schulz scans yielded intensity profiles $I(\Psi)$ representing orientation distributions of sets of lattice planes belonging to the reflection at the selected 2Θ angles relative to the AAO surface. Hence, the obtained $I(\Psi)$ profiles corresponded to azimuthal intensity profiles along the Debye ring belonging to the fixed scattering angle Θ. However, the accessible Ψ range is limited due to defocusing effects.[27] Normalized Schulz scans of the intracolumnar (001) peak for all AAO pore diameters coincided and had a full width at half-maximum of ≈8.7° (Figure 4). The steep decrease in $I(\Psi)$ shows a well-developed orientation of the (001) lattice planes normal to the AAO pore axes and, therefore, pronounced alignment of the columns with the AAO pore axes at 353 K. Hermans orientation parameter[28] amounted to ≈0.95 for all curves. Consistent with the decreasing density of the columns in the vicinity of the pore deduced from the pore diameter dependence of $T_{C_r/Col_h}$, only very weak orientation related to the intercolumnar (100) peak was detected (Figure S2, Supporting Information). Putting these findings together, a disordered (*i.e.*, defected) HBC-Br shell without preferential orientation surrounding well-ordered cores of HBC-Br columns oriented along the AAO exists, the former vanishing as the AAO pore diameter decreases. Thus, it is reasonable to assume that in smaller AAO pores with diameters of 65 nm and below the vast majority of HBC-Br molecules are incorporated in the columns aligned with the AAO pore axes (schematic diagram in Figure 3). Such configurations characterized by uniform columnar orientation in the two-dimensional confinement of self-ordered AAO are of high interest for applications in organic photovoltaics. It should be noted that in the case of smaller discotic triphenylenes confined to AAO a clear bimodal orientation distribution consisting of a core of columns oriented along the pores surrounded by a shell of columns with "homeotropic" flat-on anchoring at the AAO pore walls occurred.[19] The main difference between the triphenylenes studied previously and HBC-Br is the size of the aromatic cores. The triphenylenes can be considered as equilateral triangles with medians having a length of ∼600 nm. The aromatic cores of HBC-Br can be considered as circular disks with a diameter of ∼1120 nm that bear, in addition, five octadecyl moieties acting as spacers. It is straightforward to assume that the curvature elastic properties of both types of discotics are different and that the difference in curvature elasticity may explain why HBC-Br does, in contrast to the triphenylenes, not show bimodal orientation distributions in AAO. It is important to note that bimodal orientation distributions of discotics in AAO pores are a drawback for the functionality of supramolecular wires, for which uniform uniaxial orientation of the columns on a macroscopic scale is required. We speculate that the larger aromatic core of the HBC-Br molecules is the reason for the suppression of the formation of a distinct homeotropic shell phase. In addition, their larger core better facilitates charge transport.[4,29]

It should be noted that WAXS at 298 K confirmed the suppression of the herringbone $C_r$ phase of HNC-Br inside self-ordered AAO with diameters below 65 nm (Figure S3, Supporting Information). No pronounced orientation of HBC-Br molecules could be detected by Schulz scans taken at 298 K, even though a "precolumnar" arrangement of the HBC-Br molecules in AAO pores with diameters of 65 nm and below can be deduced from an increase in $I(\Psi)$ toward high Ψ angles apparent in Schulz scans taken at 2Θ ≈ 3.4°, corresponding to one of the prominent intercolumnar distances of the herringbone $C_r$ phase. Characteristic $I-V$ curves for HBC-Br located inside self-ordered AAO with pore diameters of 200 and 25 nm were measured at temperatures corresponding to the $Col_h$ and $C_r$ phases (Figure S5, Supporting Information). These first results reveal improved conduction properties within the $Col_h$ phase where well-ordered cores of HBC-Br columns are oriented along the AAO axes.

HBC-Br has a strong dipole directly attached to the core. Thus DS can provide not only the phase transition but also the molecular dynamics by probing the C−Br dipole.[5,9,10] Earlier investigations[5,10] in dipole-functionalized HBCs revealed a hierarchy of molecular motions that resemble the dynamics of polymers with time scales ranging from 0.01 ps to hours. In particular, concerted DS and NMR efforts[9,10] that took advantage of the strong molecular dipole and the nearby specific heteronuclear sites identified two mechanisms: a "fast" mechanism, reflecting the collective disk axial motion associated with in-plane and out-of-plane motion of the dipoles about the columnar axis that leaves an uncompensated dipole moment relaxing through the

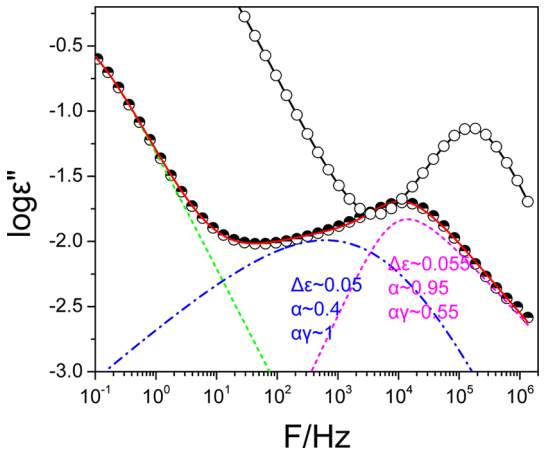


**Figure 5. Dielectric loss spectra of bulk HBC-Br (open circles) and of HBC-Br located inside self-ordered AAO with a pore diameter of 200 nm both shown at 328 K (obtained on cooling). The dashed and dash-dotted curves are the result of the fit to the Havriliak–Negami equation and correspond to the "free-rotating" and "bound" disks, respectively.**

"slower" DS process. In addition, rheology identified ultraslow cooperative defect diffusion within the $Col_h$ phase related to intercolumnar exchange.[10]

Figure 5 compares the dielectric loss spectra of bulk HBC-Br and of HBC-Br located inside self-ordered AAO with a pore diameter of 200 nm at 328 K that corresponds to the undercooled $Col_h$ phase. In bulk HBC-Br, the main process corresponds to the fast in-plane and out-of-plane motion of disks about the columnar axis. The strong increase at lower frequencies is due to a composite effect associated with the slower process and ionic conductivity.[5,9,10] In the HBC-Br located inside self-ordered AAO, dynamics is substantially different. The faster process, with low-frequency slope of $m \sim 0.9$, resembles the fast process in the bulk HBC-Br, whereas the slower process has a significantly broader distribution of relaxation times as indicated by the value of the Havriliak–Negami (HN) parameter $m \sim 0.4$. We attribute the two processes to disk dynamics in columns oriented (i) along the nanopore axis (*i.e.*, bulk-like or "free-rotating") and (ii) HBC-Br molecules located in the interphase between AAO pore walls and oriented columns (still present in AAO pores with $d = 200$ nm). As discussed above, the curvature of the AAO pore walls results in the occurrence of a distribution of packing motifs and local environments that are reflected in the low value of the HN parameter and the slower disk dynamics (as displayed in Figure S4 of the Supporting Information). At smaller pore diameters, confinement affects severely the distribution of relaxation times to a point that a deconvolution becomes ambiguous.

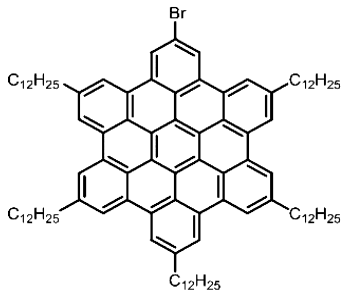


**Scheme 1. Schematic of the HBC-Br derivative.**

## CONCLUSION

Hard cylindrical confinement of rigid nanopores allows manipulating the mesoscopic self-assembly and the phase behavior of columnar discotic liquid crystals such as HBCs. Using arrays of aligned cylindrical nanopores of self-ordered AAO, uniform alignment of the columns of the model compound HBC-Br with the AAO nanopore axes could be achieved. Thus, arrays of 1D supramolecular wires with uniform columnar orientation on a macroscopic scale were realized. It could be demonstrated that larger discotics such as HBCs are particularly suitable to generate supramolecular 1D wires in the confinement of rigid nanopores. The formation of columnar HBC phases with undesired orientations is suppressed, whereas smaller discotics such as triphenylenes were reported to form columnar phases with flat-on anchoring on the AAO pore walls that impede charge transport along the wire axes. Furthermore, in larger pores a few hundred nanometers in diameter, a reduction in the $C_r/Col_h$ transition temperature was found, whereas in smaller pores, few tens of nanometers in diameter, formation of the herringbone structure was completely suppressed. On the basis of DS and DSC, the first phase diagram of a confined DLC could be derived. Finally, hard confinement of nanopores with rigid walls affects both the average time scales of disk motion and the distribution of relaxation times. These results are of technological relevance for the application of DLCs as active semiconductors in organic field-effect transistors and photovoltaic devices, where knowledge of the exact phase state and uniform columnar organization is essential.

## METHODS

**Sample:.** The synthesis of mono-bromo hexa-*peri*-hexabenzocoronene was reported previously (Scheme 1).[5] HBC-Br undergoes a first-order transformation from a low-temperature crystalline phase ($C_r$) to a liquid-crystalline high-temperature phase ($Col_h$) at 344 K with an enthalpy change of 38 J/g. On cooling from the $Col_h$ phase, the transformation to the $C_r$ phase takes place at 305 K and the associated enthalpy change is 39 J/g. In addition, HBC-Br exhibits a glass temperature at 159 K. Reagent grade dichloromethane, DCM (Sigma-Aldrich), was used as a solvent for HBC-Br and used as received.

**Infiltration of HBC-Br into Nanoporous Alumina:.** 10 mg of HBC-Br was dissolved in 50 mL of DCM, stirred at room temperature for

5 min, and subsequently sonicated in an ultrasound bath for 15 min at 313 K. The homogeneous and transparent solutions heated to 338 K were then deposited onto empty AAO membranes until a dense HBC-Br layer covered the AAO surface. The self-ordered AAO membranes infiltrated with HBC-Br were kept at 353 K ($T_{Col_h/C_r}$ + 11 K) and 200 mbar for 1 h. Afterward, excess HBC-Br was removed from the AAO surface with sharp razor blades. The amount of infiltrated HBC-Br was determined gravimetrically, and the infiltration procedure was repeated several times until the sample weight remained constant. Finally, the self-ordered AAO membranes infiltrated with HBC-Br were heated to 353 K at 100 mbar for 20 h in order remove residual DCM.

*Selective Dissolution of AAO Templates for Obtaining Free-Stading HBC-Br Nanorods:.* Free-standing HBC-Br nanorods were obtained by selective dissolution of AAO membrane using dilute $H_3PO_4$ (10%) solution at 25 °C for 3 h (Figure 1). HBC-Br nanorods were filtered off by a Sterlitech stainless steel syringe equipped with PTFE laminated membrane disk filters (pore diameter of 0.2 $\mu$m), removing the supernatant liquid, and adding deionized water. This procedure was repeated several times until the solution became neutral. Finally, nanostructures were dried in a vacuum oven at 50 °C at 100 mbar for 18 h.

**Scanning Electron Microscopy (SEM).** SEM measurements were performed with a LEO Gemini 1530 device at acceleration voltages ranging from 0.75 to 6 kV.

**Differential Scanning Calorimetry (DSC).** Thermal analyses were carried out with a Mettler Toledo Star differential scanning calorimeter (DSC) at heating and cooling rates of 10 K/min in nitrogen atmosphere. DSC traces of neat HBC-Br were acquired using an empty aluminum pan as reference. DSC traces of self-ordered AAO infiltrated with HBC-Br were recorded using reference pans containing empty AAO pieces having the same size and pore diameter. The samples were first cooled from room temperature to 153 K and then heated to 423 K. The subsequent second heating and cooling thermographs were used for the determination of phase transition temperatures and phase transition enthalpies (Figure S1).

**Wide-Angle X-ray Scattering (WAXS).** The Θ/2Θ scans were taken with a D8 Avance X-ray diffractometer (Bruker). The X-ray tube (KRISTALLOFLEX 780) generator with a Cu anode was operating at a voltage of 40 kV and a current of 30 mA. An aperture (divergence) slit of 0.3 mm, a scattered radiation (antiscatter) slit of 0.3 mm together with a monochromator slit of 0.1 mm, and a detector slit of 1 mm were employed. A diffracted beam monochromator was inserted between the detector slit and the detector to suppress fluorescence radiation and the unwanted K$\beta$ radiation. The monochromator employed a graphite crystal ($2d^* = 0.6714$ nm, for the 002 reflection). The K$\alpha$1 and K$\alpha$2 peaks could not be separated, and an average wavelength of 0.154184 nm was used. A scintillation counter with a 95% quantum yield for the Cu radiation was employed as the detector. Scans in the 2Θ range from 1 to 40° in steps of 0.01° were made at two temperatures (298 and 353 K) corresponding to the $C_r$ and $Col_h$ phases, respectively.

Schulz scans were measured with an X-ray diffractometer PANalytical X'Pert Pro MRD using Cu K$\alpha$ radiation. The samples were mounted on an Anton Paar hot stage DHS 1100 connected to an Eulerian cradle. The incident beam passed a nickel filter, a polycapillary (length 70 mm), and a cross slit collimator (slit width and height 500 $\mu$m), the diffracted beam a parallel plate collimator. The scattered intensity was detected with a PW3011/20 proportional point detector.

Schulz scans for the intercolumnar (100) peak are depicted in Figure S2. Within the experimentally accessible Ψ range from 0 to 70°, only very weak orientation related to the intercolumnar peak was detected since (100) scattering intensity belonging to the well-oriented columns aligned with the AAO pore axes would appear at Ψ ≈ 90°. In case of $d$ = 400 nm, a weak bimodal orientation distribution with maxima at Ψ ≈ 0 and 50° appeared. For $d$ = 200 nm, the peak at Ψ ≈ 0° disappeared, whereas a maximum at Ψ ≈ 50° is present. For smaller pore diameters, only an increase in $I(\Psi)$ at Ψ ≈ 60° is apparent that can be interpreted as feet of peaks appearing at Ψ ≈ 90° originating from the columns aligned with the AAO pore axes. The results from the Θ−2Θ scans at 298 K are depicted in Figure S3.

**Dielectric Spectroscopy (DS).** The dielectric measurements were performed at different temperatures in the range of 123−473 K, at atmospheric pressure, and for frequencies in the range from $10^{-2}$ to $10^6$ Hz using a Novocontrol BDS system composed of a frequency response analyzer (Solartron Schlumberger FRA 1260) and a broad-band dielectric converter and an active sample hand. For bulk HBC-Br, the DS measurements were carried out in the usual parallel plate geometry with electrodes of 20 mm in diameter and a sample thickness of 50 $\mu$m maintained by Teflon spacers. For the HBC-Br infiltrated self-ordered AAO, we used samples as those shown in the SEM images of Figure 1. In this case, the sample cell consisted of two parallel plate electrodes 20 mm in diameter with the AAO pore axes oriented perpendicular to the electrodes. The sample thickness corresponded to the pore length of ∼100 $\mu$m. The measured dielectric spectra were corrected for the geometry as follows: two capacitors in parallel composed of $\varepsilon^*_{HBC}$ and $\varepsilon^*_{AAO}$ were employed, and the measured total impedance was related to the individual values through $1/Z^*_{total} = 1/Z^*_{HBC} + 1/Z^*_{AAO}$. This allowed calculating the real and imaginary parts of the dielectric permittivity as a function of the respective volume fractions as

$$\begin{aligned} \varepsilon'_{HBC} &= \frac{\varepsilon'_{total} - \varphi_{AAO}\varepsilon'_{AAO}}{\varphi_{HBC}} \\ \varepsilon''_{HBC} &= \frac{\varepsilon''_{total}}{\varphi_{HBC}} \end{aligned} \quad (1)$$

The latter were obtained by digitization of the SEM images. There are two principal mechanisms that contribute to $\varepsilon^*$ in our case: orientation polarization of permanent dipoles ($\varepsilon^*_{dip}$) and conductivity contributions ($\varepsilon^*_{cond}$) as $\varepsilon^*(\omega,T,P) = \varepsilon^*_{dip}(\omega,T,P) - i\sigma(T,P)/(\varepsilon_f\omega)$, where $\sigma$ is the dc conductivity and $\varepsilon_f$ the permittivity of free space. The orientational contribution was fitted using the Havriliak−Negami equation

$$\varepsilon^*_{dip}(\omega, T, P) = \varepsilon_\infty(T,P) + \sum_{k=1}^{2} \frac{\Delta\varepsilon_k(T,P)}{[1+(i\omega\tau_{HN}(T,P)^{m_k}]^{n_k}} \quad (2)$$

where $\Delta\varepsilon_k(T,P)$ is the relaxation strength of the process under investigation, $\tau_{HN}$ is the relaxation time, and $m, n$ ($0 < m, mn \leq 1$) describe the symmetrical and asymmetrical broadening of the distribution of relaxation times, and $\varepsilon_\infty(T,P)$ is the dielectric permittivity at the limit of high frequencies. The relaxation times at maximum loss ($\tau_{max}$) are presented herein and have been analytically obtained from the Havriliak−Negami equation as follows:

$$\left[\sin\left(\frac{\pi m}{2+2n}\right)\right]^{1/m} \tau_{max} = \tau_{HN}\left[\sin\left(\frac{\pi mn}{2+2n}\right)\right]^{1/m} \quad (3)$$

The relaxation times at maximum loss are summarized in Figure S4.

*Conflict of Interest:* The authors declare no competing financial interest.

*Acknowledgment.* G.F. acknowledges support during his sabbatical leave at the MPI-P. The current work was supported by the Research unit on Dynamics and Thermodynamics of the UoI co-financed by the European Union and the Greek state under NSRF 2007-2013 (Region of Epirus, call 18) and the operational program of the NSRF "Aristeia". H.D. and M.S. gratefully acknowledge financial support from the German Research Foundation (SPP 1369, BU 1556/31-1, STE 1127/13, and INST 190/134-1). The preparation of AAO by C. Hess and H. Tobergte and SEM investigations by G. Glasser are gratefully acknowledged.

*Supporting Information Available:* DSC cooling and subsequent heating thermograms of bulk HBC-Br and of HBC located inside self-ordered AAO with pore diameters ranging from 200 to 25 nm, Schulz scans at 353 K, Θ−2Θ scans at 298 K, temperature dependence of the disk dynamics in bulk HBC-Br and in HBC-Br located inside self-ordered AAO, and $I-V$ characteristic

curves for two AAO pore sizes. This material is available free of charge *via* the Internet at http://pubs.acs.org.

## REFERENCES AND NOTES


1. Adam, D.; Schuhmacher, P.; Simmerer, J.; Haussling, L.; Siemens-Meyer, K.; Etzbach, K. H.; Ringsdorf, H.; Haarer, D. Fast Photoconduction in the Highly Ordered Columnar Phase of a Discotic Liquid Crystal. *Nature* **1994**, *371*, 141–143.
2. van de Craats, A. M.; Warman, J. M.; Fechtenkötter, A.; Brand, J. D.; Harbison, M. A.; Müllen, K. Record Charge Carrier Mobility in a Room-Temperature Discotic Liquid-Crystalline Derivative of Hexabenzocoronene. *Adv. Mater.* **1999**, *11*, 1469–1472.
3. Pisula, W.; Menon, A.; Stepputat, M.; Lieberwirth, I.; Kolb, U.; Tracz, A.; Sirringhaus, H.; Pakula, T.; Müllen, K. A Zone-Casting Technique for Device Fabrication of Field-Effect Transistors Based on Discotic Hexa-*peri*-hexabenzocoronene. *Adv. Mater.* **2005**, *17*, 684–689.
4. Feng, X.; Marcon, V.; Pisula, W.; Hansen, M. R.; Kirkpatrick, J.; Grozema, F.; Andrienko, D.; Kremer, K.; Müllen, K. Towards High Charge-Carrier Mobilities by Rational Design of the Shape and Periphery of Discotics. *Nat. Mater.* **2009**, *8*, 421–426.
5. Haase, N.; Grigoriadis, C.; Butt, H.-J.; Müllen, K.; Floudas, G. Effect of Dipole Functionalization on the Thermodynamis and Dynamics of Discotic Liquid Crystals. *J. Phys. Chem. B* **2011**, *115*, 5807–5814.
6. Grigoriadis, C.; Haase, N.; Butt, H.-J.; Müllen, K.; Floudas, G. Negative Thermal Expansion in Discotic Liquid Crystals of Nanographenes. *Adv. Mater.* **2010**, *22*, 1403–1406.
7. Grigoriadis, C.; Haase, N.; Butt, H.-J.; Müllen, K.; Floudas, G To Tilt or Not to Tilt? Kinetics of Structure Formation in a Discotic Liquid Crystal. *Soft Matter* **2011**, *7*, 4680–4689.
8. Papadopoulos, P.; Grigoriadis, C.; Haase, N.; Butt, H.-J.; Müllen, K.; Floudas, G. Dynamics of Structure Formation in a Discotic Liquid Crystal by Infrared Spectroscopy and Related Techniques. *J. Phys. Chem. B* **2011**, *115*, 14919–14927.
9. Elmahdy, M. M.; Floudas, G.; Mondeshki, M.; Spiess, H. W.; Dou, X.; Müllen, K. Origin of the Complex Molecular Dynamics in Functionalized Discotic Liquid Crystals. *Phys. Rev. Lett.* **2008**, *100*, 107801-4.
10. Hansen, M. R.; Feng, X.; Macho, V.; Müllen, K.; Spiess, H. W.; Floudas, G. Fast and Slow Dynamics in a Discotic Liquid Crystal with Regions of Columnar Order and Disorder. *Phys. Rev. Lett.* **2011**, *107*, 257801-4.
11. Masuda, H.; Fukuda, K. Ordered Metal Nanohole Arrays Made by a Two-Step Replication of Honeycomb Structures of Anodic Alumina. *Science* **1995**, *268*, 1466–1468.
12. Masuda, H.; Hasegwa, F.; Ono, S. Self-Ordering of Cell Arrangement of Anodic Porous Alumina Formed in Sulfuric Acid Solution. *J. Electrochem. Soc.* **1997**, *144*, L127–L130.
13. Masuda, H.; Yada, K.; Osaka, A. Self-Ordering of Cell Configuration of Anodic Porous Alumina with Large-Sized Pores in Phosphoric Acid Solution. *Jpn. J. Appl. Phys.* **1998**, *37*, L1340–L1342.
14. Steinhart, M. Supramolecular Organization of Polymeric Materials in Nanoporous Hard Templates. *Adv. Polym. Sci.* **2008**, *220*, 123–187.
15. Duran, H.; Gitsas, A.; Floudas, G.; Mondeshki, M.; Steinhart, M.; Knoll, W. Poly($\gamma$-benzyl-L-glutamate) Peptides Confined to Nanoporous Alumina: Pore Diameter Dependence of Self-Assembly and Segmental Dynamics. *Macromolecules* **2009**, *42*, 2881–2885.
16. Grigoriadis, C.; Duran, H.; Steinhart, M.; Kappl, M.; Butt, H.-J.; Floudas, G. Suppression of Phase Transitions in a Confined Rodlike Liquid Crystal. *ACS Nano* **2011**, *5*, 9208–9215.
17. Duran, H.; Steinhart, M.; Butt, H.-J.; Floudas, G. From Heterogeneous to Homogeneous Nucleation of Isotactic Poly(propylene) Confined to Nanoporous Alumina. *Nano Lett.* **2011**, *11*, 1671–1675.
18. Kopitzke, J.; Wendorff, J. H.; Glüsen, B. Columnar Discotics in Confined Geometries. *Liq. Cryst.* **2000**, *27*, 643–648.
19. Steinhart, M.; Zimmermann, S.; Göring, P.; Schaper, A. K.; Gösele, U.; Weder, C.; Wendorff, J. H. Liquid Crystalline Nanowires in Porous Alumina: Geometric Confinement *versus* Influence of Pore Walls. *Nano Lett.* **2005**, *5*, 429–434.
20. Pisula, W.; Kastler, M.; Wasserfallen, D.; Davies, R. J.; Garcia-Gutiérrez, M.-C.; Müllen, K. From Macro- to Nanoscopic Templating with Nanographenes. *J. Am. Chem. Soc.* **2006**, *128*, 14424–14425.
21. Mouthuy, P.-O.; Melinte, S.; Geerts, Y. H.; Jonas, A. M. Uniaxial Alignment of Nanoconfined Columnar Mesophases. *Nano Lett.* **2007**, *7*, 2627–2632.
22. Floudas, G. Dielectric Spectroscopy. In *Polymer Science: A Comprehensive Reference*; Matyjaszewski, K., Möller, M., Eds.; Elsevier BV: Amsterdam, 2012; Vol. 2.32, pp 825–845.
23. Diez-Berart, S.; Lopez, D. O.; de la Fuente, M. R.; Salud, J.; Perez-Jubindo, M. A.; Finotello, D. Critical Behaviour at Liquid-Crystalline Phase Transitions. A Comparative Study of 9OCB in Bulk and Anopore Membranes. *Liq. Cryst.* **2010**, *37*, 893–901.
24. Perez-Jubindo, M. A.; de la Fuente, M. R.; Diez-Berart, S.; Lopez, D. O.; Salud, J. Influence of Cylindrical Submicrometer Confinement on the Static and Dynamic Properties in Nonyloxycyanobiphenyl (9OCB). *J Phys. Chem. B* **2008**, *112*, 6567–6577.
25. Schulz, L. G. A Direct Method of Determining Preferred Orientation of a Flat Reflection Sample Using a Geiger Counter X-ray Spectrometer. *J. Appl. Phys.* **1949**, *20*, 1030–1032.
26. Steinhart, M.; Göring, P.; Dernaika, H.; Prabhukaran, M.; Gösele, U.; Hempel, E.; Thurn-Albrecht, T. Coherent Kinetic Control over Crystal Orientation in Macroscopic Ensembles of Polymer Nanorods and Nanotubes. *Phys. Rev. Lett.* **2006**, *97*, 027801-4.
27. Chernock, W. P.; Beck, P. A. Analysis of Certain Errors in the X-ray Reflection Method for the Quantitative Determination of Preferred Orientations. *J. Appl. Phys.* **1952**, *23*, 341–345.
28. Hermans, P. H.; Vermaas, D.; Weidinger, A. Quantitative Evaluation of Orientation in Cellulose Fibres from the X-ray Fibre Diagram. *Rec. Trav. Chim.* **1946**, *65*, 427–447.
29. van de Craats, A. M.; Warman, J. M. The Core-Size Effect on the Mobility of Charge in Discotic Liquid Crystalline Materials. *Adv. Mater.* **2001**, *13*, 130–133.